ELSEVIER

Journal of Alloys and Compounds 235 (1996) 156–162

Journal of ALLOYS AND COMPOUNDS

Luminescent europium–dibenzoylmethane complexes and their Langmuir–Blodgett films

Dejian Zhou[a], Chunhui Huang[a,*], Guangqing Yao[a], Jie Bai[b], Tiankai Li[b]

[a]*State Key Laboratory of Rare Earth Material Chemistry and Applications, Peking University, Beijing 100871, People's Republic of China*
[b]*Institute of Photographic Chemistry, Academia Sinica, Beijing 100101, People's Republic of China*

Received 7 September 1995; in final form 2 November 1995

Abstract

Two strong fluorescent amphiphilic europium–dibenzoylmethane complexes, hexadecyltrimethyl ammonium tetrakis (dibenzoylmethane) europium (**A**) and octadecyltriethyl ammonium tetrakis (dibenzoylmethane) europium (**B**), were synthesized and characterized by FT-IR, UV–vis, DTA–TG analysis and X-ray diffraction. Both of them could form stable Langmuir films at the air–water interface and the Langmuir film of **A** can be easily transferred onto hydrophilic substrates to build up Langmuir–Blodgett (LB) films. The LB film of **A** has a good layered structure, as confirmed by its low-angle X-ray diffraction. The fluorescence spectra and fluorescence lifetimes of the LB films were quite different from those of their corresponding solid powders and solutions.

Keywords: Rare earth fluorescence complexes; Europium; Langmuir–Blodgett films

1. Introduction

Rare earth fluorescence complexes have been of great interest owing to their characteristic high fluorescence efficiency, good fluorescence monochromaticity, very narrow fluorescence band and potential applications for optical devices [1,2]. Recent studies show that some rare earth complexes can form stable Langmuir films at the air–water interface, and their Langmuir films can be easily transferred onto solid substrates to form good quality Langmuir–Blodgett (LB) films [3–10]. By combining the LB technique with strong fluorescence lanthanide complexes, highly homogenized strongly luminescent ultrathin films could be obtained [7–10]. These fluorescent LB films may have special use in microcavity applications, which may have important use in thresholdless laser oscillation [11,12].

However, only those complexes which have good performance both in fluorescence and Langmuir film formation and transformation can be used. To provide fundamental data for this aspect, some exploratory work has been done which showed that the Eu–PMBP complex (PMBP = 1-phenyl-3-methyl-4-benzoyl-pyrazoyl-5-one) has good film stability and transferability, but it has relatively poor fluorescence performance [13,14]. On the contrary, the Eu–TTA complexes (TTA = 2-thenoyltrifluoro-acetone) have good fluorescence intensity, but they were unable to form stable Langmuir films [7] or they have a very low transfer ratio; the addition of matrix molecules is needed to obtain their LB films [8,9]. In this paper, two strongly fluorescent europium–dibenzoylmethane complexes $Me_3NC_{16}H_{33} \cdot Eu(DBM)_4$ (**A**) and $Et_3NC_{18}H_{37} \cdot Eu(DBM)_4$ (**B**), whose molecular structures are depicted in Fig. 1, were synthesized. Their

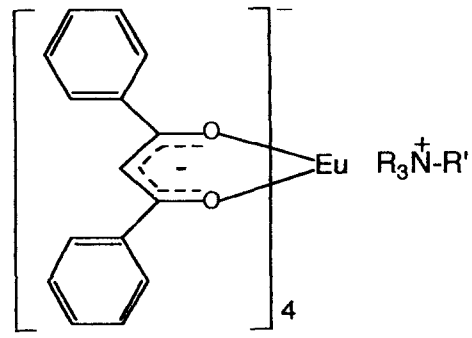

Fig. 1. Molecular structures of compound **A** (R = Me, R' = $C_{16}H_{33}$) and **B** (R = Et, R' = $C_{18}H_{37}$).

* Corresponding author.

SSDI 0925-8388(95)02159-0

Langmuir films at the air–water interface and the deposition of the monolayers to form LB films were investigated. Their fluorescence spectra and fluorescence lifetimes of the LB films were examined and compared with those of the solutions and solid powders.

2. Experimental

2.1. Materials and synthesis

Eu_2O_3 (greater than 99.9%) was purchased from Yuelong Chemical Factory (Shanghai, People's Republic of China). Dibenzoyl methane (HDBM, C.P. grade) was bought from Beijing Chemical Factory (Beijing, People's Republic of China). Hexadecyl trimethyl ammonium bromide (HTMAB) and octadecyltriethyl ammonium bromide (OTEAB) were A.R. grade products from Beijing Chemical Factory (Beijing, People's Republic of China). The europium perchlorate $Eu(ClO_4)_3$ aqueous solution was prepared by dissolving Eu_2O_3 with perchloric acid to get a concentration of 0.40 M, pH = 4.0. Other reagents were all A.R. grade chemicals from Beijing Chemical Factory.

The compounds **A** and **B** were prepared in a similar way. A brief preparation for **A** is described as follows [13]. 4.4 mmol HDBM and 1.00 mmol HTMAB were dissolved in 40 ml ethanol under heating, then 4.00 mmol NaOH aqueous solution was added and a yellowish solution was obtained. After that, 1.00 mmol $Eu(ClO_4)_3$ aqueous solution was added dropwise and a yellowish precipitate was formed. The crude precipitate was filtered and collected when the mixture cooled to room temperature, then it was recrystallized in mixed solvents of ethanol–acetone (1:1) and yellowish needle crystals were obtained. Compound **A** was obtained by filtration and dried at 70°C for 2 h.

Compound **A**, m.p. 163–164°C. Anal. Found: C, 71.37; H, 6.67; Eu, 11.36; N, 0.82. $C_{79}H_{86}EuNO_8$. Calc.: C, 71.20; H, 6.73; Eu, 11.41; N, 1.05%. Compound **B**, m.p. 152–153°C. Anal. Found: C, 71.74; H, 7.07; Eu, 11.06; N, 0.77. $C_{84}H_{96}EuNO_8$. Calc.: C, 72.10, H, 6.92; Eu, 10.87; N, 1.00%.

2.2 Instruments and measurements

IR spectra of HDBM and the complexes were recorded on a Magna 750 FT-IR spectrophotometer, using KBr pellets in the range of 4000–400 cm^{-1}. Thermoanalysis was measured on a LCT-1 type DTA and TG analyser system under air atmosphere. α-Al_2O_3 was used as the reference and the temperature was raised at a rate of 10°C min^{-1}. The UV–vis spectra were recorded on a Shimadazu UV-3100 spectrophotometer at a slit width of 2 nm. Low-angle diffractograms were obtained on a Rigaku D/Max-3B diffractometer, using Cu Kα radiation ($\lambda = 0.154$ nm). Fluorescence excitation and emission spectra were recorded on a Hitachi 850 fluorescence spectrophotometer, using a 430 nm excitation cutoff filter. Excitation and emission bandwidths of 5 nm were employed and the fluorescence spectra were corrected for nonlinear instrumental response and blank solvents.

The fluorescence lifetime determination was performed on an SLM 48000 Multi-Frequency Phase Fluorometer, using the frequency-domain method with glycogen as the reference [15]. A 580 nm long-pass filter was placed in the emission path to eliminate the interference from the solvent and stray light. The modulated frequency used ranges from 200 to 5000 Hz. At each frequency, both the phase shift and the relative modulation values were measured six times and the average values were used to evaluate the fluorescence lifetime in order to minimize the experimental error. A total of ten different frequencies were used, and the final fluorescence lifetime was determined by least squares analysis of the data, leading to a minimum value of R [16–19].

$$R = (1/2)\left\{\sum_{\omega}[(\phi_\omega - \phi^c_\omega)/\delta_\phi]^2 + \sum_{\omega}[(M_\omega - M^c_\omega)/\delta_M]^2\right\} \quad (1)$$

where ϕ_ω and ϕ^c_ω are the measured and the calculated phase shift, M_ω and M^c_ω are the measured and the calculated modulation, and δ_ϕ and δ_M are the average phase error (0.5°) and modulation error (0.005).

A NIMA Langmuir trough was used for the Langmuir–Blodgett study. The Langmuir films of **A** and **B** were formed by carefully depositing their corresponding $CHCl_3$ solutions (ca. 1 g l^{-1}) on pure water subphase (20 ± 1°C, pH = 5.60). After allowing the solvent to evaporate for 20 min, the floating films were compressed at a rate of 20 mm min^{-1} and the surface pressure–area (π–A) isotherms were recorded. The monolayer of **A** was transferred onto a hydrophilically pretreated [3] fused quartz Y-type plate at a dipping speed of 10 mm min^{-1}. During the Langmuir film transfer procedure, the surface pressure was always kept within 15.0 ± 0.1 mN m^{-1} and the transfer ratio was found to be always around unity.

3. Results and discussion

3.1. IR spectra and thermostability

There is only one strong carbonyl stretching peak at 1598 cm^{-1} in the HDBM ligand, indicating that two carbonyl groups are connected by the intra-molecular

hydrogen bonding [20,21]. Compounds **A** and **B** also show a strong carbonyl stretching peak at 1599 cm^{-1}, just like the free ligand. However, another new strong peak at 1518 cm^{-1} occurs in both of the complexes. This is the characteristic C=C stretching peak of the DBM ligand coordinating with the central Eu(III) ion in the form of an alkenol anion [22]. The broad strong stretching peak of the phenyl ring at 1550 cm^{-1} in HDBM blue shifts about 5 cm^{-1} in the complexes. Some new peaks at 2925 and 2853 cm^{-1} appear in the complexes, which can be assigned to the asymmetric and symmetric stretching of the CH_2 group in the long chains of the complexes [20].

The DTA–TG curves of **A** and **B** are similar. They are both chemically stable from room temperature to 230°C. There are no changes in their TG curves, but their DTA curves both exhibit a sharp endothermic peak (163°C for **A**, 152°C for **B**), corresponding to their melting points. Their TG curves exhibit a relatively large weight loss in the range 230–330°C, and the DTA curves both show a broad exothermic band. This process is considered to be the complexes losing their ammonium salt and a DBM ligand forming $Eu(DBM)_3$ [23,24]. The weight loss percentages (experimental/theoretical) are 44.8/38.2% for **A** and 45.2/41.4% for **B**. In the 330–550°C region, they both undergo a series of complicated oxidation and decomposition reactions and finally form Eu_2O_3 [24]. The DTA curves have a large exothermic band and the TG curves exhibit a series of weight losses. There are no changes in either the TG or DTA curves when the temperature is higher than 550°C. The overall weight loss percentages are 86.2/86.7% for **A** and 86.8/87.4% for **B**. The experimental values are in fairly good agreement with the theoretical ones. This indicates that they are both thermally stable enough to be used for further application in molecular devices.

3.2. Surface pressure–area isotherms

The surface pressure–area (π–A) isotherms of the Langmuir films of **A** and **B** are similar and are shown in Fig. 2. They both show only one solid phase which collapses at around a surface pressure of 27 mN m^{-1}. The slope of the solid phase for **A** (0.70 mN m^{-1} $Å^{-2}$) is bigger than that for **B** (0.39 mN m^{-1} $Å^{-2}$), and the limiting area, obtained by extrapolation of the rising portion of the isotherm to $\pi = 0$, for **A** (0.96 nm^2/molecule) is smaller than that for **B** (1.38 nm^2/molecule). This indicates that the **A** molecules can pack much closer and are much more easily orderly arranged at the air–water interface than **B**. Using crystal structure parameters of a similar model complex, $Et_3NH \cdot Eu(DBM)_4$ [25], we calculated the limiting area for the $Eu(DBM)_4^-$ complex anion to be 1.00 nm^2/molecule, in good agreement with the value

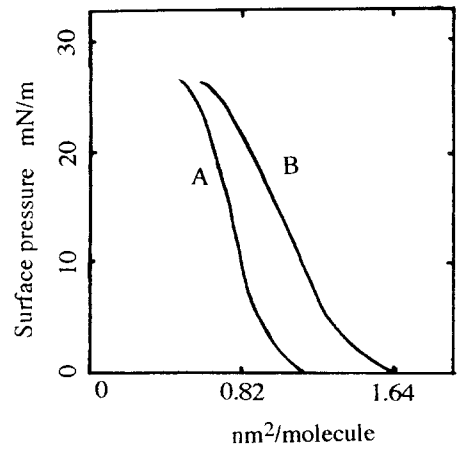

Fig. 2. Surface pressure–area isotherms of the Langmuir films of **A** and **B** at the air–water interface.

obtained from the π–A isotherm of **A**. This indicates that the area of the Langmuir films occupied at the air–water interface is mainly controlled by the $Eu(DBM)_4^-$ complex anion. This can be rationalized as the large complex anions being closely pack at the interface, while the hydrophilic terminals of the long chain ammonium ion stand in the voids formed by the complex anion [6]. In compound **A**, the hydrophilic Me_3N–R terminal is small, so that the complex anion could pack closely, thus the limiting area almost equals that of the $Eu(DBM)_4^-$ complex anion; but, in compound **B**, the larger hydrophilic Et_3N–R′ terminal prevents the complex anion from close packing, so the limiting area obtained from the isotherm is bigger. The Langmuir films of **A** can be readily transferred onto hydrophilic quartz substrates with a transfer ratio around unity. However, the transfer ratio for the Langmuir film of **B** decreases significantly as the layer number increases, maybe due to its smaller slope of the solid phase.

3.3. UV–vis spectra and low-angle X-ray diffraction

The UV–vis spectra of the HDBM in $CHCl_3$, compound **A** in $CHCl_3$ and a 19-layered LB film of **A** are shown in Fig. 3. The UV–vis spectrum of the HDBM ligand in $CHCl_3$ solution shows two broad absorption bands at 253 ($\varepsilon = 4800$ M^{-1} cm^{-1}) and 343 nm ($\varepsilon = 1.26 \times 10^4$ M^{-1} cm^{-1}), assignable to the $\pi \rightarrow \pi^*$ electronic transfer on the phenyl ring and carbonyl group [26,27]. The UV spectra of **A** and **B** in $CHCl_3$ also exhibit two absorption bands. The former band shows no change, but the later one red-shifts about 2–3 nm, indicating that the DBM ligand forms a bigger conjugate system after coordination with the europium ion. The two bands both strengthened significantly. Their molar absorption coefficients both

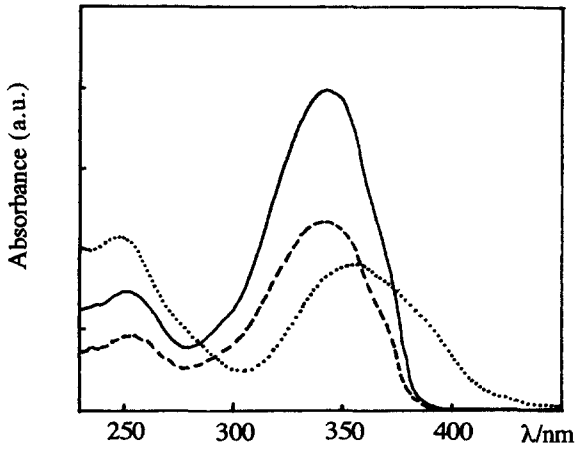

Fig. 3. UV–vis spectra of HDBM in $CHCl_3$ (broken line), compound **A** in $CHCl_3$ (solid line) and a 19-layer LB film of **A** on a quartz substrate (dotted line).

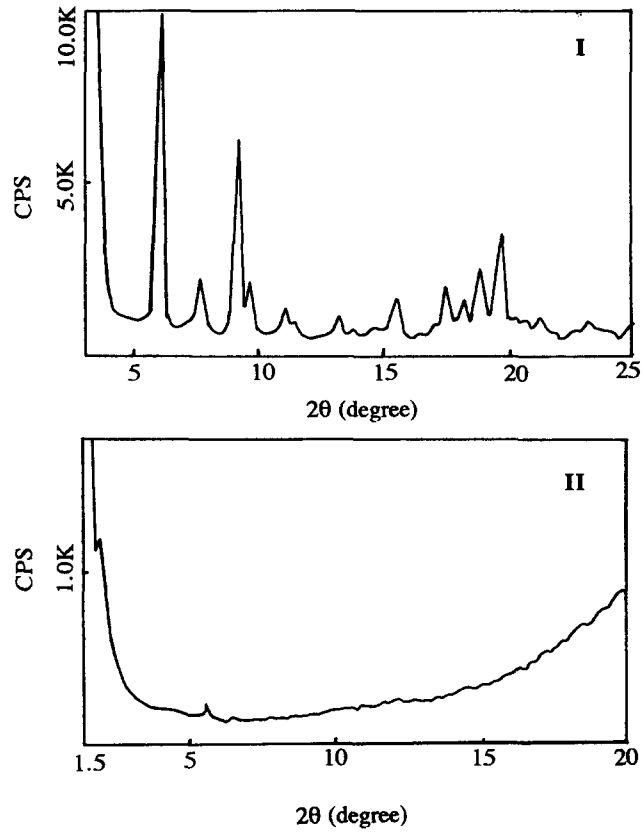

Fig. 4. Low-angle X-ray diffractograms of the powder complex of **A** (I) and a 19-layer LB film on a quartz substrate (II).

enlarge to be 3.8×10^4 M^{-1} cm^{-1} for the former and 1.00×10^5 M^{-1} cm^{-1} for the latter; both are about seven times stronger than those in the free ligand. The LB film for **A** also shows two broad bands around 253 and 355 nm. The latter band red-shifts about 10 nm, while the former remains unchanged compared with the complex in $CHCl_3$ solution. The relative intensities of the two bands are almost identical in the LB films, quite different from that of the $CHCl_3$ solution. These changes maybe due to the intermolecular electronic transfer in the two dimensional orderly arranged molecules in the LB films [17].

The X-ray powder diffractograms of **A** and **B** both show several diffraction peaks. The diffractogram of **A** is shown in Fig. 4. Using the well-known Bragg equation, the crystalline distances of the major diffraction peaks are obtained and given as follows (Å(relative intensity)): compound **A**, 14.36(100), 11.47(21), 9.55(61), 9.06(21), 8.00(13), 6.68(11), 5.69(16), 5.07(20), 4.87(16), 4.70(24), 4.50(34), 4.39(11), 4.29(10), 4.19(11), 3.83(10); compound **B**, 14.48(100), 12.44(33), 9.60(64), 8.84(16), 8.54(16), 5.73(34), 5.38(13), 5.26(16), 4.92(21), 4.82(41), 4.70(23), 4.55(20), 4.09(17), 3.94(12), 3.87(13), 3.65(11). The low-angle X-ray diffractogram of a 19-layered LB film of compound **A** on a quartz plate is significantly different from that of its powder complex (Fig. 4). It shows two weak but evident diffraction peaks at 2θ 1.90 and 5.68°, revealing a well-defined film structure. The two peaks are assigned to the (001) and (003) Bragg diffraction. The average double-layer spacing of 4.66 nm is thus obtained according to the Bragg equation, and this yields the single-layer film thickness of 2.33 nm based on the Y-type LB film structure (one double-layer contains two single layers). The distance is in fairly good agreement with the calculated value of 2.26 nm based on that of the long chain of the vertically arranged ammonium. This regular X-ray diffraction pattern indicates that the LB film has a highly ordered layer structure [5].

3.4. Fluorescence spectra

The two complexes are strongly fluorescent in the solid state, in $CHCl_3$ solution or in ordered LB films. However, the excitation and emission spectra are quite different for the three states, as shown in Figs. 5 and 6. Some fluorescence data are listed in Table 1. The excitation spectra of solid powders both show a wide band from 200 to 400 nm. The excitation intensity decreases slightly with the exciting wavelength. In the $CHCl_3$ solution, it has a weak broad band around 300 nm and a much stronger band around 415 nm. The excitation intensity is much weaker than that of solid powder (about 1/100). This may be due to the small concentration of the solution (ca. 1 mM) and the interaction between the fluorescent complex and the solvent molecules. There are two broad excitation bands around 260 and 356 nm in the 19-layer LB film of **A**. Both the position of the excitation bands and the shape of the spectrum are quite different compared with those of the solid powder or $CHCl_3$ solution,

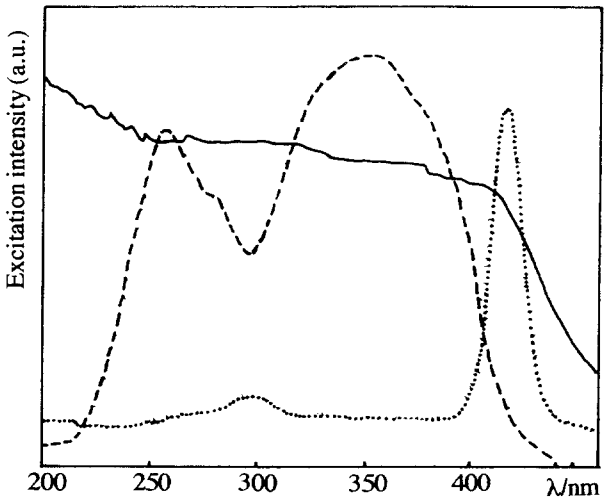

Fig. 5. Fluorescence excitation spectra of compound **A** at different states. Solid powder (solid line), $CHCl_3$ solution (dotted line) and 19-layer LB film (broken line).

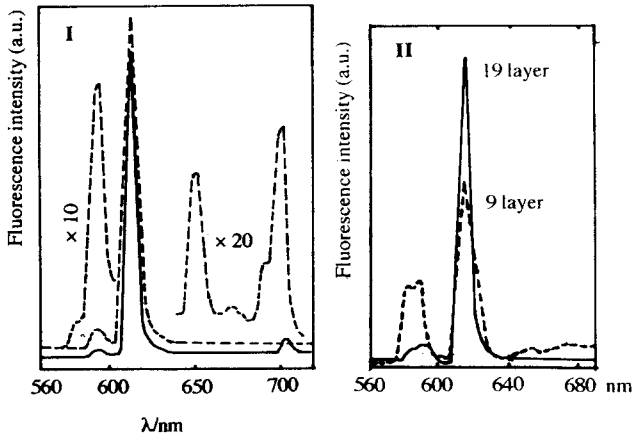

Fig. 6. Fluorescence spectra of **A** at different state. . (I) Solid powder (solid line) and $CHCl_3$ solution (broken line). (II) 19-layer (solid line) and 9-layer LB films on quartz plates.

possibly because of the different molecular orientations in the three states [10].

The emission spectra from the LB films, $CHCl_3$ solution and solid powder are all characteristic for Eu(III), which can be attributed to the $^5D_0 \rightarrow {}^7F_j$ (j = 0, 1, 2) electronic transitions. The electric dipolar $^5D_0 \rightarrow {}^7F_2$ transition is the strongest, and then the magnetic $^5D_0 \rightarrow {}^7F_1$ transition. However, the shapes of the fluorescence spectra and the ratios of the relative intensity between the electric dipolar transition ($^5D_0 \rightarrow {}^7F_2$) and magnetic transition ($^5D_0 \rightarrow {}^7F_1$) ($I_{ED}/I_{MD}$) are quite different. These values are listed in Table 2. The powder complex has the biggest I_{ED}/I_{MD} value and the LB film has the smallest. This may be due to the different coordination symmetry of the central Eu^{3+} in the different states [28]. The powder complex has the smallest symmetry, while the LB film has the best. It is noteworthy that I_{ED}/I_{MD} in the 9-layered LB film is only 2.2, but it increases to 18 in 19-layered LB films, comparable with the values in solutions, indicating that the coordination symmetry of Eu^{3+} decreases as the layer number increases. Similar results have been observed by Qian et al. [9]; the fluorescence intensity of the $^5D_0 \rightarrow {}^7F_1$ transition was almost the same as that of the $^5D_0 \rightarrow {}^7F_2$ transition in the mixed monolayer film of $Me_2N(C_{18}H_{37})_2 \cdot Eu(TTA)_4$ and arachidic acid (1:16). The fluorescence intensity of the 19-layered LB film is 1.14 times stronger than that of the 9-layer film. This linear enhanced fluorescence intensity with the layer number, reflects the effective transfer of the Langmuir films.

3.5. Fluorescence lifetime

Owing to the time lag between absorption and emission, the emission is delayed for the modulated excitation. The fluorescence lifetime could be evaluated by measuring the phase shift and the relative modulation of the samples at different modulated excitation frequency. The basic equations in the frequency-domain method for determining the fluorescence lifetime are as follows [15]:

$$\tau_\phi = \tan \phi/\omega \quad (2)$$

where ϕ is the phase shift caused by a sample of lifetime τ_ϕ, and ω is the circular frequency of excitation (equal to 2π times the excitation frequency in hertz);

Table 1
Comparison of the fluorescence spectra of **A** and **B** in the $CHCl_3$ solution and LB films

State	Excitation	Emission $^5D_0 \rightarrow {}^7F_j$ position (intensity)				
	Peak position	$j=0$	$j=1$	$j=2$	$j=3$	$j=4$
Solution **A**	300(7.5) 415(67)	580(0.10)	594(1.00)	614(19.5)	652(0.3)	693(0.16) 703(0.4)
Solution **B**	300(10) 416(71)	580(0.11)	593(1.00)	614(19.7)	652(0.3)	692(0.16) 702(0.4)
9-layer **A**	260(44) 360(75)	583(0.90)	590(1.00)	615(2.2)	652(0.2)	
19-layer **A**	260(62) 356(77)	582(0.60)	592(1.00)	614(18)		

The fluorescence intensity is normalized by each one's magnetic ($^5D_0 \rightarrow {}^7F_1$) transition.

Table 2
Fluorescence comparison of the complexes in the three different states

State	λ_{max}^{EX} (nm)	λ_{max}^{EM} (nm)	Relative intensity	I_{ED}/I_{MD}	τ (μs)
A (solid)	365	614.4	1400	58	360 ± 10
B (solid)	365	613.5	3900	37	460 ± 10
A ($CHCl_3$)	414	612.8	12.1	19.5	86 ± 5
B ($CHCl_3$)	414	612.5	12.3	19.7	84 ± 5
A (acetone)	418	613.1	21.1	18.7	139 ± 10
A (DMF)	418	613.4	22.5	19.0	144 ± 10
A (toluene)	418	613.2	23.4	18.5	107 ± 5
A (CH_3CO_2Et)	418	613.3	20.6	18.4	102 ± 10
A (9-layer LB film)	355	614.7	1.0	2.2	—
A (19-layer LB film)	356	614.0	2.1	18	146 ± 25

The concentrations of the solutions were all 1 mM.

$$\tau_M = (1/\omega)[(1/D^2) - 1]^{0.5} \quad (3)$$

where D is the ratio of the relative modulation of the fluorescent sample and the glycogen reference solution.

By measuring the phase shift and the relative modulation of the samples at different frequency and using the methods described above, least squares analysis of the data showed that the fluorescence lifetimes of **A** and **B** are different at different states and they are given in Table 2. All the samples exhibit only one fluorescent component and a typical example of the lifetime determination of **A** is shown in Fig. 7.

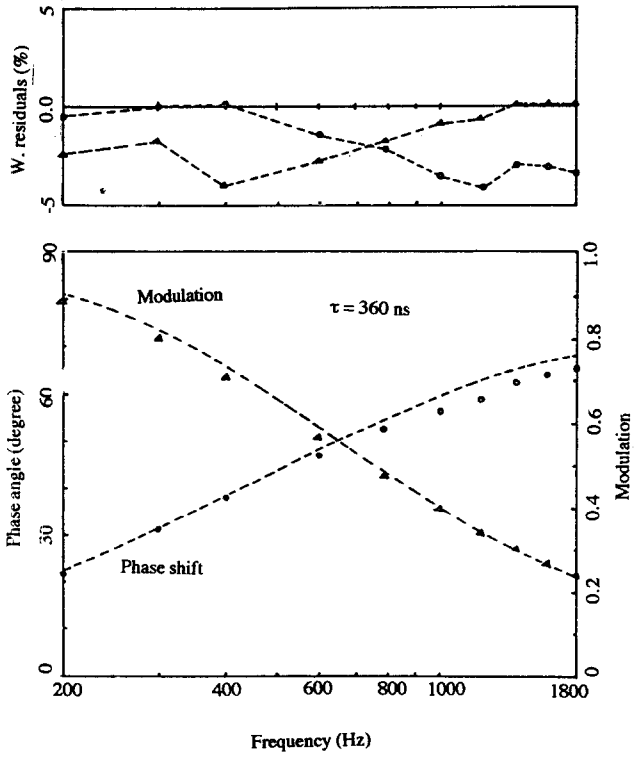

Fig. 7. A typical example of determination of the fluorescence lifetime of **A** in the solid state using the frequency-domain method. Open circles and triangles are the measured phase shifts and modulations; the dashed lines show the best fit with a single decay time.

The fluorescence lifetimes of **A** and **B** in the solid state are much longer than their corresponding solutions or LB films, and the values agree with the earlier results quite well. For example: 414 μs for $C_5H_{12} \cdot Eu(DBM)_4$ crystal at 300 K [29]. It is interesting that both the fluorescence intensity and the fluorescence lifetime of the solid powder of **B** are respectively much stronger and longer than that of **A**, reflecting that the fluorescence efficiency of **B** powder is much higher than **A**. This indicates that the counter ammonium ions strongly affect the luminescent properties of the complexes. However, both the fluorescence intensity and lifetime of **A** and **B** are almost identical in $CHCl_3$ solutions, and the values are highly comparable with the value of $C_5H_{12} \cdot Eu(DBM)_4$ in EPA (97 μs, EPA = 3:3:1(v/v) diethyl ether–isopentane–ethanol) [29]. The fluorescence lifetimes of the solutions differ significantly from solvent to solvent; the longest is exhibited in DMF and the shortest in $CHCl_3$ among the five solvents studied. This may be due to the different ion pairing state in different solutions and the different fluorescence quenching ability of the solvents. The fluorescence lifetime of the LB film is longer than most of the solutions but significantly shorter than its powder complex; this may be the result of the different symmetry of the Eu^{3+} coordination environment in the three states. The possibility for the thermal deactivation of the excited state in solutions is much bigger than that in LB films, and thus the fluorescence lifetime in LB film is longer.

4. Conclusions

In summary, we prepared two strong luminescent europium complexes $Me_3NC_{16}H_{33} \cdot Eu(DBM)_4$ (**A**) and $Et_3NC_{18}H_{37} \cdot Eu(DBM)_4$ (**B**) which can form stable Langmuir films at the air–water interface. High quality LB films of **A** were obtained by the conventional LB technique (vertical dipping method). The fluorescent intensity and fluorescence lifetime are quite different for different states and show strong

solvent dependence in solution. The powder complex has the strongest fluorescence intensity and the longest fluorescence lifetime, while the solution has the shortest fluorescence lifetime. This provides valuable data for the application of fluorescent lanthanide-complex LB films in microcavity laser oscillations. The good Langmuir film formation and transformation property of **A** makes it more suitable for such a study, because its film thickness can be precisely controlled at the single molecular layer level (the most important requirement for microcavity lasers). Further work is in progress to use the luminescent LB film of **A** in microcavities.

Acknowledgements

The authors thank the Climbing Program (A National Fundamental Research Key Project of the People's Republic of China) and the National Natural Science Foundation the People's Republic of China for financial support.

References

[1] T. Moeller and E. Schleitzer-Rust (eds.), *Gmelin Handbook of Inorganic Chemistry*, Part D3, Springer, Berlin, 1981, 8th edn., pp. 65–246.
[2] L.R. Melby, N.J. Rose, E. Abramson and J.C. Caris, *J. Am. Chem. Soc.*, *86* (1964) 5117.
[3] C.H. Huang, X.Y. Zhu, K.Z. Wang, G.X. Xu, Y. Xu, Y.Q. Liu, P. Zhang and X.P. Wang, *Chin. Chem. Lett.*, *2* (1991) 741.
[4] D.J. Zhou, C.H. Huang, K.Z. Wang, G.X. Xu, X.S. Zhao, X.M. Xie, L.G. Xu and T.K. Li, *Langmuir*, *10* (1994) 1910.
[5] K.Z. Wang, C.H. Huang, G.X. Xu, Y. Xu, Y.Q. Liu, D.B. Zhu, X.S. Zhao, X.M. Xie and N.Z. Wu, *Chem. Mater.*, *6* (1994) 1986.
[6] H. Li, C.H. Huang, G.X. Xu, X.S. Zhao, X.M. Xie, L.G. Xu and T.K. Li, *Langmuir*, *10* (1994) 3794.
[7] K.Z. Wang, C.H. Huang, G.Q. Yao, G.X. Xu, D.F. Cui and Y. Fan, *Chem. J. Chin. Univ.*, *14* (1993) 150 (in Chinese).
[8] D.J. Qian and K.Z. Yang, *Acta Phys. Chem. Sin.*, *9* (1993) 148 (in Chinese).
[9] D.J. Qian, H. Nakahara, K. Fukuda and K.Z. Yang, *Chem. Lett.*, (1995) 175.
[10] D.J. Zhou, K.Z. Wang, C.H. Huang, G.X. Xu, L.G. Xu and T.K. Li, *Solid State Commun.*, *93* (1995) 167.
[11] M. Suzuki, H. Yokoyama, S.D. Brorson and E.P. Ippen, *Appl. Phys. Lett.*, *58* (1991) 998.
[12] A. Dodabalapur, L.J. Rothberg, T.M. Miller and E.W. Kwock, *Appl. Phys. Lett.*, *64* (1994) 2486.
[13] D.J. Zhou, *Ph.D. Thesis*, Department of Chemistry, Peking University, 1995.
[14] C.H. Huang, K.Z. Wang, X.Y. Zhu, G.X. Xu, Y. Xu, Y.Q. Liu, P. Zhang and X.P. Wang, *Solid State Commun.*, *90* (1994) 151.
[15] J.R. Lakowicz and I. Gryczynski, in J.R. Lakowicz (ed.), *Topics in Fluorescence Spectroscopy*, Vol. 1, Plenum, New York, 1991.
[16] D.J. Zhou, H.S. Tan, L.B. Gan, C.P. Luo, C.H. Huang and G.Q. Yao, *Chem. Lett.*, (1995) 649.
[17] D.J. Zhou, G.Q. Yao, C.H. Huang, J. Bai and T.K. Li, *Chin. Chem. Lett.*, *6* (1995) 903.
[18] D.J. Zhou, L.B. Gan, H.S. Tan, C.P. Luo, C.H. Huang and G.Q. Yao, *Chem. J. Chin. Univ.*, *16* (1995) 1512 (in Chinese).
[19] D.J. Zhou, L.B. Gan, H.S. Tan, C.P. Luo, C.H. Huang, G.Q. Yao and P. Zhang, *Chin. Sci. Bull.*, in press (in Chinese).
[20] J.X. Xie, *Application of IR Spectra in Organic and Pharmaceutical Chemistry*, Science Press, Beijing, 1987 pp. 158–160 (in Chinese).
[21] C.Y. Liang, E.J. Schimitschek and J.A. Trias, *J. Inorg. Nucl. Chem.*, *32* (1970) 811.
[22] D.J. Zhou, C.H. Huang, G.Q. Yao, Y.F. Zhou, J. Bai and T.K. Li, *J. Chin. Rare Earth Soc.*, *13* (1995) 193 (in Chinese).
[23] S.L. Lyle and A.D. Witts, *Inorg. Chim. Acta*, *5* (1971) 481.
[24] A. Perotto and R.G. Charles, *J. Inorg. Nucl. Chem.*, *26* (1964) 373.
[25] L.M. Sweeting and A.L. Rheingold, *J. Am. Chem. Soc.*, *109* (1987) 2652.
[26] L. Huang and D.Q. Yu, *Application of UV Spectra in Organic Chemistry*, Science Press, Beijing, 1988.
[27] D. Purushottam, V.R. Rao and B.S.V. Raghava Rao, *Anal. Chim. Acta*, *33* (1965) 182.
[28] W.X. Hou, Y.R. Wang, Y.B. Bai, Z.Q. Zhu, T.J. Li and Y.N. Zhao, *Spectrosc. Spectro Anal.*, *6* (3) (1986) 25 (in Chinese).
[29] M.L. Bhaumik and L.J. Nugent, *J. Chem. Phys.*, *43* (1965) 1680.